Article

Photoproduction of Loop Currents in Coronene Isomers Without Any Applied Magnetic Field

Jun Ohara *[ID] **and Shoji Yamamoto**[ID]

Department of Physics, Hokkaido University, Sapporo 060-0810, Japan; yamamoto@phys.sci.hokudai.ac.jp
* Correspondence: ohara@phys.sci.hokudai.ac.jp

Abstract: Applying an extended Peierls–Hubbard model to π electrons in a coronene isomer, we investigate their ground-state properties and photoinduced dynamics with particular interest in possible loop current states. Once we switch on a static magnetic field perpendicular to the coronene disk, diamagnetic (diatropic) and paramagnetic (paratropic) loop currents appear on the rim circuit and inner hub, respectively. Besides this well-known homocentric two-loop current state, heterocentric multiloop current states can be stabilized by virtue of possible electron–lattice coupling. These multiloop current states generally have a larger diamagnetic moment than the conventional two-loop one, and hence it follows that coronene, or possibly polycyclic conjugated hydrocarbons in general, may become more aromatic than otherwise with their π electrons being coupled to phonons. When we photoirradiate a ground-state coronene isomer without applying a static magnetic field, loop currents are induced in keeping with the incident light polarization. Linearly and circularly polarized lights induce heterocentric two-loop and multiloop currents, respectively, without and together with two homocentric loop currents of the conventional type, respectively. The heterocentric two-loop currents occur in a mirror-symmetric manner, which reads as the emergence of a pair of antiparallel magnetic moments, whereas the heterocentric multiloop ones appear at random in both space and time, which reads as the emergence of disordered local magnetic moments.

Keywords: polycyclic aromatic hydrocarbon; coronene; loop current; photoinduced dynamics

1. Introduction

Ring currents in conjugated π-electron systems are closely related to their aromaticity [1,2]. In monocyclic systems, aromatic compounds with $4n + 2$ π electrons (n: integer) exhibit a diamagnetic current, whereas antiaromatic compounds with $4n$ π electrons show a paramagnetic current [3]. These π-electron ring currents can be observed through nuclear magnetic resonance spectroscopy [4,5]. In polycyclic systems, the classification of ring currents is not as simple as in monocyclic systems. The interplay of geometric structures, electronic structures, and molecular vibration modes causes a novel response to a magnetic field.

Coronene of chemical formula $C_{24}H_{12}$ [6] is a chemically stable and highly symmetric polycyclic conjugated hydrocarbon, which has six centrosymmetrically edge-sharing benzene hexagons assembled in a concentric disk (Figure 1a). Its zigzag perimeter and internal hexagon have 18 and 6 π electrons, respectively, each satisfying the aromatic Hückel count $4n + 2$ and therefore implying conrotatory diamagnetic currents emergent along the outer and inner circumferences. However, nucleus-independent chemical-shift observations [7] and density functional calculations [8,9] both claim that coronene isomers have diamagnetic outer and paramagnetic inner circuits. Graphical [10] and further density functional [11,12] investigations demonstrate various lattice vibration modes as well as ring current patterns. In addition, potassium (K)-doped coronene exhibits superconductivity with its critical temperature amounting to 15 K [13–16]. The electronic properties of coronene and related polyaromatic hydrocarbons [17] are thus multifunctional and therefore attractive.

In recent years, photoinduced ring currents in aromatic molecules have been attracting considerable attention from the viewpoint of coherent control of electric currents, where simple and small molecules, such as benzene [18], Na$_{10}$ rings [19], and (*P*)-2,2'-biphenol [20], have been investigated based on time-dependent density functional approaches. In such circumstances, we focus on photoexcited coronenes in an attempt to obtain new insights into dynamic ring currents in polycyclic aromatic compounds. First, we investigate possible electronic states, including ring current states, of coronene based on an extended Peierls–Hubbard model. The interplay of an electron–lattice (el) coupling and Coulomb interactions is discussed using ground-state phase diagrams with and without an applied static magnetic field. Second, we simulate the photoirradiation of coronenes with linearly and circularly polarized lights, and observe the induced electric currents, electric polarizations, and optical conductivities. We find new loop current structures that never appear under the applied static magnetic field, and demonstrate photomanipulation of the electric circulations by the polarization of light, which leads to the new development of organic optoelectronic devices.
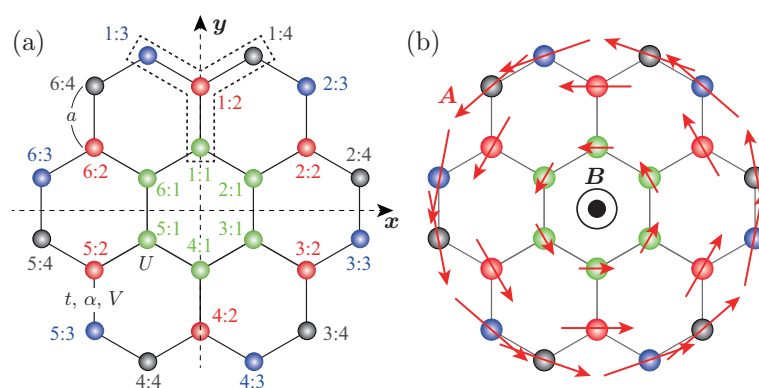

Figure 1. (**a**) A coronene isomer with physical parameters t (bare transfer integral), α (electron–lattice coupling), U (on-site Coulomb repulsion), V (inter-site Coulomb repulsion), and a (distance between adjacent carbon atoms). Green, red, blue, and gray circles indicate the 1st-, 2nd-, 3rd-, and 4th-site carbons, respectively, in a Y-shaped unit. (**b**) The vector potential $A \equiv (-yB/2, xB/2, 0)$ induces a static magnetic field, $B = (0, 0, B)$.

2. Model Hamiltonian

Employing a half-filled extended Peierls–Hubbard Hamiltonian, we describe π electrons on a coronene molecule:

$$\mathcal{H} = -\sum_{l=1}^{6}\sum_{\sigma=\uparrow,\downarrow}\Big[t_{l+1:1,l:1}c^{\dagger}_{l+1:1,\sigma}c_{l:1,\sigma} + t_{l:2,l:1}c^{\dagger}_{l:2,\sigma}c_{l:1,\sigma} + t_{l:3,l:2}c^{\dagger}_{l:3,\sigma}c_{l:2,\sigma}$$

$$+ t_{l:4,l:2}c^{\dagger}_{l:4,\sigma}c_{l:2,\sigma} + t_{l+1:3,l:4}c^{\dagger}_{l+1:3,\sigma}c_{l:4,\sigma} + \text{h.c}\Big] + U\sum_{l=1}^{6}\sum_{i=1}^{4}n_{l:i,\uparrow}n_{l:i,\downarrow}$$

$$+ V\sum_{l=1}^{6}\Big(n_{l+1:1}n_{l:1} + n_{l:2}n_{l:1} + n_{l:3}n_{l:2} + n_{l:4}n_{l:2} + n_{l+1:3}n_{l:4}\Big)$$

$$+ \frac{K}{2}\sum_{l=1}^{6}\Big(y^{2}_{l+1:1,l:1} + y^{2}_{l:2,l:1} + y^{2}_{l:3,l:2} + y^{2}_{l:4,l:2} + y^{2}_{l+1:3,l:4}\Big), \tag{1}$$

$$t_{m:j,l:i} = t\exp\left[-i\frac{e}{\hbar c}\int_{\boldsymbol{r}_{l:i}}^{\boldsymbol{r}_{m:j}} \boldsymbol{A}(\boldsymbol{r})\cdot d\boldsymbol{r}\right] - \alpha y_{m,j,l:i}, \tag{2}$$

where $n_{l:i} \equiv \sum_{\sigma=\uparrow,\downarrow} n_{l:i,\sigma} \equiv \sum_{\sigma=\uparrow,\downarrow} c^{\dagger}_{l:i,\sigma}c_{l:i,\sigma}$ is the occupation operator with $c^{\dagger}_{l:i,\sigma}$ creating a σ-spin electron at the i-th ($i = 1$ to 4)-site carbon in the l-th ($l = 1$ to 6) unit indicated by $\boldsymbol{r}_{l:i}$ (Figure 1a). A periodic boundary condition along the circumferential direction is imposed as $c^{\dagger}_{7:i,\sigma} = c^{\dagger}_{1:i,\sigma}$, $y_{7,j,6:i} = y_{1,j,6:i}$, and $\boldsymbol{r}_{7:i} = \boldsymbol{r}_{1:i}$. We introduce the vector potential

$A(\boldsymbol{r})$ by multiplying the electron hopping t by a Peierls phase factor as in Equation (2), where α and $y_{m:j,l:i}$ denote an el coupling and a lattice displacement between the j-th-site carbon in the m-th unit [$(m:j)$ carbon] and the i-th-site carbon in the l-th unit [$(l:i)$ carbon], respectively. On-site and inter-site Coulomb repulsions are denoted as U and V, respectively, and a spring constant is given by K. In the present study, a numerical diagonalization is conducted by using the LAPACK (version 3.2) subroutine ZHEEV.

3. Ground-State Phase Varieties and Their Optical Features

The possible electronic states of coronene in the absence and presence of a static magnetic field are discussed within a Hartree–Fock (HF) scheme [21,22]. The lattice displacements are determined so as to minimize the ground-state energy under the conditions $\sum_{l=1}^{6} y_{l+1:1,l:1} = 0$, $\sum_{l=1}^{6} y_{l+1:2,l:2} = 0$, and $\sum_{l=1}^{6} (y_{l:3,l:2} + y_{l:4,l:2} + y_{l+1:3,l:4}) = 0$, which conserve the lengths of the hub and rim circumferences, and the volume of the molecule. We consider the z-direction uniform magnetic field, which is induced by the vector potential presented in Figure 1b. When $B = 0$, the point-group symmetry of the Hamiltonian is $\mathbf{D}_{6h}$. Figure 2a shows a ground-state phase diagram with no magnetic field. A bond-order-wave (BOW) state with full symmetry of the Hamiltonian predominates in a moderate el-coupling and Coulomb-interaction regime. With reference to the parameters for poly-acetylene ($t = 2.5$ eV, $\alpha = 4.1$ eV/Å, $K = 21$ eV/Å^2, $\alpha/\sqrt{Kt} = 0.56$, and $U/t \simeq 1$) [23–25], BOW is likely to be a candidate for a realistic ground state [11]. With increasing Coulomb interactions and el coupling, a charge density wave (CDW) in the y direction (y-CDW) and a CDW in the x direction (x-CDW) appear, respectively, as broken symmetry solutions [26]. In addition, charge polarization (CP) in the x and y directions, abbreviated as x-CP and y-CP, respectively, are induced by the strong el coupling. Such a charge-polarized state exists as a broken symmetry solution in platinum-halide ladder compounds as well [27]. However, it never becomes a true ground state because Peierls-distorted states are more stable in quasi-one-dimensional systems. In contrast, CP in coronene possibly occurs spontaneously without any applied external field.

Once a magnetic field is applied, the point-group symmetry of the Hamiltonian is reduced to $\mathbf{C}_{6h}$, and the time-reversal symmetry is broken. The static magnetic field induces various ring current states as is shown in Figure 2b. In the moderate el-coupling and Coulomb-interaction regime, a two-loop current (2-LC) state, with full symmetry of the Hamiltonian under a magnetic field, appears. The inner and outer currents are paramagnetic and diamagnetic, respectively. In our calculations, the paramagnetic current is sufficiently smaller than the diamagnetic one, which is consistent with previous work [8–10]. The other kinds of loop current states, the four-loop current (4-LC) and five-loop current (5-LC) states, are stabilized by the strong el coupling. These multiloop current states appear as broken symmetry solutions with $\mathbf{C}_{3h}$ symmetric lattice distortions. These lattice distortions make the effective transfer integral nonuniform and bring about the heterocentric multiloop currents. In comparison with the conventional homocentric 2-LC state, the 5-LC state has three more diamagnetic circuits, and the 4-LC state has three more diamagnetic circuits and no paramagnetic circuit. Since two-loop currents on the rim circuits and inner hub are almost the same among the 5-LC, 4-LC, and 2-LC states, the diamagnetic currents simply increase in the heterocentric loop structures. Then, diamagnetic moments in the 5-LC and 4-LC states are about 14 percent and 15 percent, respectively, larger than those in the 2-LC state. Thus, the coronene with sufficiently strong el coupling, possibly with heterocentric multiloop currents, shows higher aromaticity. In kekulene, consisting of twelve annelated benzene rings, for example, heterocentric multiloop currents actually appear in response to a uniform magnetic field [28]. The Coulomb interactions do not change the loop current structure, but simply bring about the CDW structure.
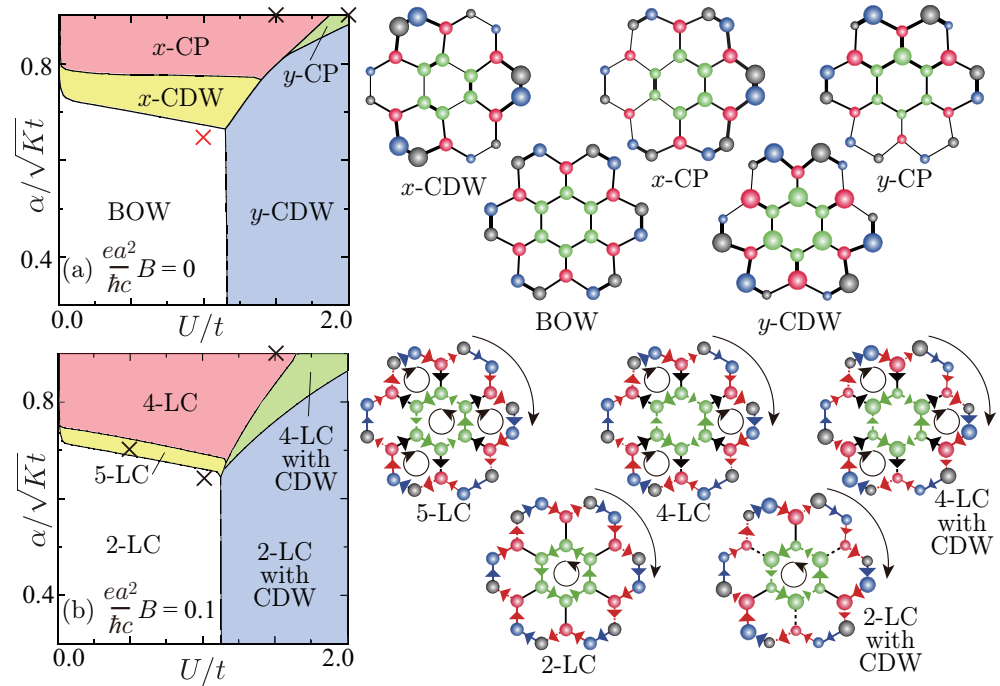
Figure 2. Ground-state phase diagrams on a *U*-*α* plane in the absence (**a**) and presence (**b**) of the static magnetic field, where *V* is set to 0.7*U*. Possible electronic states are also illustrated, where the size of circles denotes the amount of electron densities and the round arrows indicate loop currents. The symbols × point to $(U/t, \alpha/\sqrt{Kt}) = (1.0, 0.64)$ for BOW, $(1.5, 0.90)$ for *x*-CP, $(2.0, 0.90)$ for *y*-CP, $(1.0, 0.64)$ for 2-LC, $(0.5, 0.70)$ for 5-LC, and $(1.5, 0.90)$ for 4-LC, which are the parameter points of the electronic states in the investigation of optical conductivities (Figure 3). In particular, the red cross indicates the initial BOW state in the investigation of photoinduced dynamics.
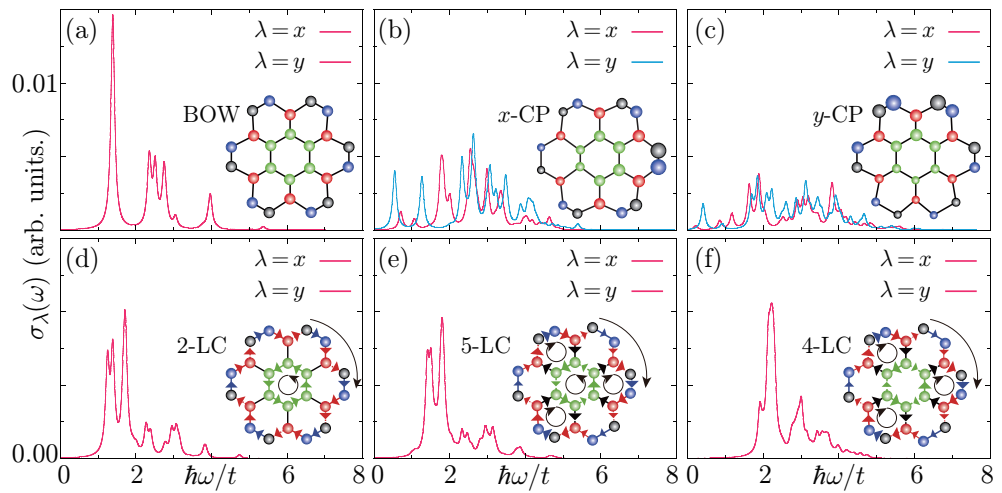

Figure 3. Polarized optical conductivities in the absence [(**a**) BOW, (**b**) *x*-CP, and (**c**) *y*-CP] and presence [(**d**) 2-LC, (**e**) 5-LC, and (**f**) 4-LC] of the static magnetic field.

Let us observe the ground-state optical conductivity spectra $\sigma_\lambda(\omega)$ ($\lambda = x, y$) of several electronic phases [29],

$$\sigma_\lambda(\omega) = \frac{\pi}{\omega} \sum_\mu |\langle E_\mu | J_\lambda | E_0 \rangle|^2 \delta(E_\mu - E_0 - \hbar\omega), \tag{3}$$

where $|E_\mu\rangle$ is the μ-th one-electron–hole-pair excited state from the ground state $|E_0\rangle$, and the current-density operator $J = (J_x, J_y, 0)$ is defined as

$$J = \sum_{l=1}^{6} (j_{l+1:1,l:1} + j_{l:2,l:1} + j_{l:3,l:2} + j_{l:4,l:2} + j_{l+1:3,l:4}), \tag{4}$$

$$j_{m:j,l:i} = j_{m:j,l:i} \frac{(r_{m:j} - r_{l:i})}{|r_{m:j} - r_{l:i}|};$$

$$j_{m:j,l:i} = -i\frac{ea}{\hbar} \sum_{\sigma=\uparrow,\downarrow} (t_{m:j,l:i} c_{m:j,\sigma}^{\dagger} c_{l:i,\sigma} - \text{H.c.}). \tag{5}$$

The optical conductivity (Equation (3)) is defined as a response to an external electric field within a linear response theory [30]. It corresponds to the current–current correlation function, which tells us the photoabsorption spectrum of electronic systems [31].

Figure 3 presents the thus-obtained polarized optical conductivities. The energy gap of the BOW state (Figure 3a) is 3.0 eV when $t = 2.5$ eV, which is consistent with the energy gap of 2.9 eV obtained by density functional theory [14]. There exist three well-defined energy bands. In the electrically polarized states, x-CP (Figure 3b) and y-CP (Figure 3c) states, the degeneracy of $\sigma_x(\omega)$ and $\sigma_y(\omega)$ is lifted. Their oscillator strengths are continuously distributed over the low-energy and high-energy regions in comparison with those of the BOW state. In the presence of the magnetic field (Figure 3d–f), all the loop current states show optical gaps, and the oscillator strengths decrease gradually from the low-energy to high-energy regions, at a glance. The spectra of the 2-LC and 5-LC states seem to be almost the same, but that of the 5-LC is slightly shifted toward a higher-energy region. The spectrum of the 4-LC state with no paramagnetic circuit is obviously distributed in a higher-energy region in comparison with that of the 2-LC state. With an increase in the aromaticity, the optical conductivity spectrum is blue-shifted. The loop current states as well as the BOW state have rotational symmetry around the principal (z) axis (the BOW and 2-LC states are invariant to the C_6 and C_3 rotations, while the 4-LC and 5-LC states are invariant to the C_3 one). In such a rotationally symmetric state, a center of electric charge is located at the origin, and therefore, it shows the isotropic response to an external electric field (Figure 3a,d–f), unlike the electrically polarized states (Figure 3b,c).

4. Light-Polarization-Dependent Dynamic Loop Currents

We consider the photoexcitation of the initial BOW state. Electron and lattice dynamics of photoexcited coronene are investigated by solving the time-dependent Schrödinger equation [32,33]:

$$i\hbar \frac{d}{d\tau} |\Psi_{\nu,\sigma}(\tau)\rangle = \mathcal{H}_{\text{HF}}(\tau) |\Psi_{\nu,\sigma}(\tau)\rangle, \tag{6}$$

where $|\Psi_{\nu,\sigma}(\tau)\rangle$ ($\nu = 1, 2, \cdots, 24; \sigma = \uparrow, \downarrow$) is the one-particle wavefunction for a σ-spin electron on the ν-th energy level at time τ, which at $\tau \to -\infty$ corresponds to the ν-th eigenstate of the static HF Hamiltonian. The lattice displacement between carbons in this two-dimensional system is evaluated as

$$y_{m:j,l:i} \simeq \frac{(r_{m:j} - r_{l:i}) \cdot (u_{m:j} - u_{l:i})}{|r_{m:j} - r_{l:i}|}, \tag{7}$$

where $u_{l:i}$ is a displacement of the ($l:i$) carbon from its equilibrium position $r_{l:i}$. We treat the lattice vibrations classically and consider the time evolution of the classical value $u_{l:i}$ based on the equation of motion:

$$M \frac{d^2}{d\tau^2} u_{l:i} = -\frac{\partial \langle \mathcal{H}_{\text{HF}}(\tau) \rangle}{\partial u_{l:i}} [\equiv F(\tau)], \tag{8}$$

where the mass of the carbon atom M is set to 1349.14 eVfs^2/Å^2 [34], and $\langle \cdots \rangle$ is an expectation value in the state $|\Psi(\tau)\rangle = \Pi_{\nu=1}^{12} \Pi_{\sigma=\uparrow,\downarrow} \otimes |\Psi_{\nu,\sigma}(\tau)\rangle$. $|\Psi(-\infty)\rangle$ corresponds to the initial BOW state. Discretizing the time by $\Delta\tau$, we numerically integrate Equations (6) and (8) step by step. The electronic part is solved as

$$
\begin{aligned}
|\Psi_{\nu,\sigma}(\tau + \Delta\tau)\rangle &= \mathcal{T} \exp\left[-\frac{i}{\hbar} \int_{\tau}^{\tau+\Delta\tau} d\tau' \mathcal{H}_{\mathrm{HF}}(\tau')\right] |\Psi_{\nu,\sigma}(\tau)\rangle \\
&\simeq \exp\left[-\frac{i}{\hbar} \mathcal{H}_{\mathrm{HF}}(\tau)\Delta\tau\right] |\Psi_{\nu,\sigma}(\tau)\rangle \\
&= \sum_{\nu'=1}^{24} \sum_{\sigma'=\uparrow,\downarrow} \exp\left[-\frac{i}{\hbar} \varepsilon_{\nu',\sigma'}\Delta\tau\right] |\phi_{\nu',\sigma'}\rangle \langle \phi_{\nu',\sigma'}|\Psi_{\nu,\sigma}(\tau)\rangle,
\end{aligned}
\tag{9}
$$

where $\mathcal{T}$ is the time-ordering operator, while $\varepsilon_{\nu',\sigma'}$ and $|\phi_{\nu',\sigma'}\rangle$ denote the eigenvalue and eigenfunction of the instantaneous Hamiltonian $\mathcal{H}_{\mathrm{HF}}(\tau)$, respectively. Here, we note that $\sum_{\nu'=1}^{24} \sum_{\sigma'=\uparrow,\downarrow} |\phi_{\nu',\sigma'}\rangle \langle \phi_{\nu',\sigma'}| = 1$. The equation of motion for the lattice displacement $\{u_{l:i}\}$ (Equation (8)) is a second-order differential equation and is treated as the simultaneous first-order differential equations for $\{u_{l:i}\}$ and $\{\dot{u}_{l:i}\}$:

$$
M\frac{d}{d\tau}\dot{u}_{l:i} = F(\tau), \quad \frac{d}{d\tau}u_{l:i} = \dot{u}_{l:i}.
\tag{10}
$$

Based on a standard Euler method, we obtain the time evolution of the lattice part as

$$
\begin{aligned}
u_{l:i}(\tau + \Delta\tau) &= u_{l:i}(\tau) + \dot{u}_{l:i}(\tau)\Delta\tau, \\
\dot{u}_{l:i}(\tau + \Delta\tau) &= \dot{u}_{l:i}(\tau) + \frac{F(\tau)}{M}\Delta\tau,
\end{aligned}
\tag{11}
$$

where $\Delta\tau$ is set to $5 \times 10^{-4} \omega_Q^{-1} = 5 \times 10^{-4}\sqrt{M/2K}$. We describe a pumping laser pulse by the vector potential

$$
\begin{aligned}
A(\tau) &= [A_x(\tau), A_y(\tau), 0]; \\
A_x(\tau) &= A_0 e^{-\gamma^2(\tau-\tau_0)^2} \cos\theta \cos\omega_0\tau, \\
A_y(\tau) &= A_0 e^{-\gamma^2(\tau-\tau_0)^2} \sin\theta \cos(\omega_0\tau - \kappa\pi/2),
\end{aligned}
\tag{12}
$$

where $\hbar\omega_0$ is the photon energy. When we set κ equal to zero and unity, Equation (12) yields linearly and circularly polarized lights, respectively. The applied dynamic electric field is given by $E(\tau) = -(1/c)dA(\tau)/d\tau$. The pumping photon energy $\hbar\omega_0$ is set to the optical gap energy of the initial BOW state, while A_0, γ^{-1}, and τ_0 are set to $0.04\hbar c/ea$, $14\omega_Q^{-1}$, and $20\omega_Q^{-1}$, respectively.

To observe photoinduced loop currents, we calculate the electric currents along the perimeter of the individual benzene ring and rim of the coronene molecule:

$$
J_0(\tau) = \frac{1}{6}\sum_{l=1}^{6} \langle j_{l+1:1,l:1}\rangle,
\tag{13}
$$

$$
\begin{aligned}
J_l(\tau) = \frac{1}{6}\langle &j_{l:2,l:1} + j_{l:4,l:2} + j_{l+1:3,l:4} + j_{l+1:2,l+1:3} \\
&+ j_{l+1:1,l+1:2} + j_{l:1,l+1:1}\rangle \quad (l = 1 \text{ to } 6),
\end{aligned}
\tag{14}
$$

$$
J_7(\tau) = \frac{1}{18}\sum_{l=1}^{6} \langle j_{l:2,l:3} + j_{l:4,l:2} + j_{l+1:3,l:4}\rangle,
\tag{15}
$$

where J_0, J_l ($l = 1$ to 6), and J_7 correspond to the center benzene, surrounding six benzenes, and rim components, respectively. The electric polarization

$$\boldsymbol{P}(\tau) = [P_x(\tau), P_y(\tau), 0] = \sum_{l=1}^{6} \sum_{i=1}^{4} \langle n_{l:i} \rangle \boldsymbol{r}_{l:i} \tag{16}$$

is also monitored in the time evolution of the electronic state.

Let us overview the photoinduced electron dynamics of coronene in Figure 4. In the case of photoirradiation with $\theta = 0$ linearly polarized light (Figure 4a–c), loop currents do not emerge along the internal hexagon or along the zigzag perimeter, unlike the magnetic-field-induced ring current states. The second and fifth benzene rings on the x axis also show no loop current, but the first, third, fourth, and sixth benzene rings, located perpendicular to the direction of the electric field, show the circulations of electrons. The electric polarization in the x direction (P_x) is also induced by the laser pumping. In the case of photoirradiation with $\theta = \pi/6$ linearly polarized light (Figure 4a′–c′), both the J_0 and J_7 components are zero as in the case of $\theta = 0$, but the other loop current components, J_l ($l = 1$ to 6), are observed. Regarding the electric polarization, P_x and P_y appear in phase with each other, while the magnitude of the induced polarization is smaller than that in the $\theta = 0$ case. The linearly polarized light induces neither J_0 nor J_7. On the other hand, all the loop current components, including J_0 and J_7, are induced by the circularly polarized light with $\theta = \pi/4$ (Figure 4a″–c″). The oscillations of the induced P_x and P_y show asynchronicity originating from the phase difference in the applied electric field.
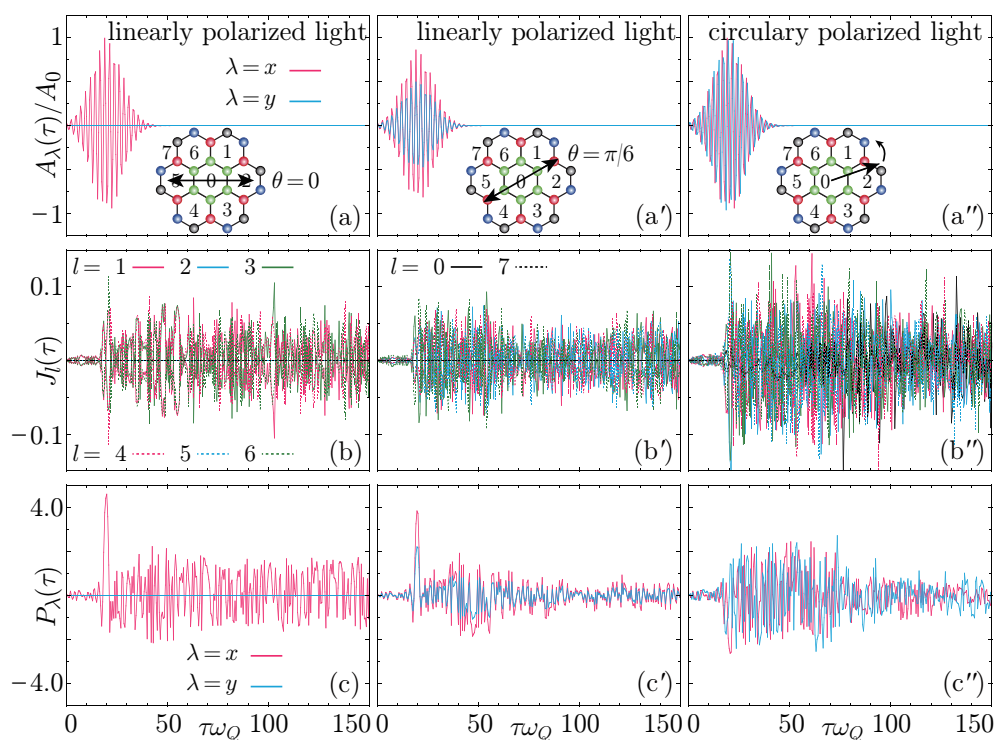

Figure 4. The vector potentials $A(t)$ for linearly polarized light with $\theta = 0$ (**a**) and $\theta = \pi/6$ (**a′**) and circularly polarized light with $\theta = \pi/4$ (**a″**). The time evolutions of the induced loop currents [(**b**), (**b′**), and (**b″**)] and electric polarizations [(**c**), (**c′**), and (**c″**)] are presented.

Figure 5 presents the details of the dynamical electric currents and polarizations after laser pumping. First, we focus on the loop currents induced by the linearly polarized light with $\theta = 0$ (Figure 5a). In Figure 5a, J_1 (red solid line) and J_6 (green dotted line) almost always show the same sign, i.e., the same direction of circulation (see, for example, around $\tau \omega_Q = 102$ and 114.5). In this sense, the electric circulations on the adjacent first

and sixth benzene rings occur in phase with each other, and form a one large loop current. Such a composite loop current appears on the adjacent third and fourth benzene rings as well. These two loop currents are in mirror symmetry with respect to the *z-x* plane. In Figure 5b, P_x is generated when the loop currents temporarily disappear. In other words, the heterocentric two-loop currents and electric polarization appear alternately in time. Figure 6a,b show the optical conductivities at $\tau\omega_Q = 101$ and 111, respectively. A difference between σ_x and σ_y, which is a characteristic of the CP states, is observed in Figure 6a, whereas a gradual decrease in oscillator strength from the low-energy to high-energy regions, which is a characteristic of the ring current states, is seen in Figure 6b.
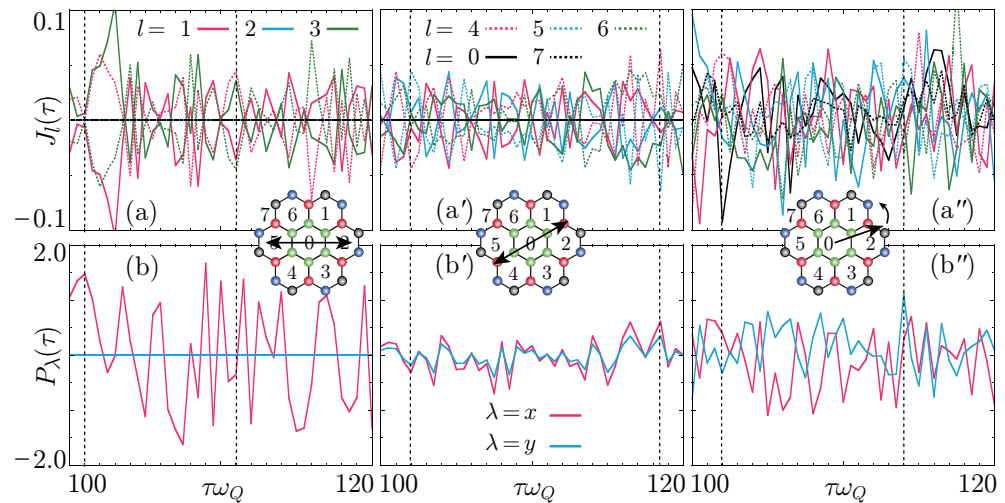

Figure 5. Dynamic loop currents (**the upper panels**) and electric polarizations (**the lower panels**) in the range of $100 \leq \tau\omega_Q \leq 120$, which are induced by the photoirradiations with linearly polarized light with $\theta = 0$ (**a**,**b**) and $\theta = \pi/6$ (**a′**,**b′**) and circularly polarized light with $\theta = \pi/4$ (**a″**,**b″**). We calculate optical conductivities at the times indicated by vertical dotted lines (see Figure 6).

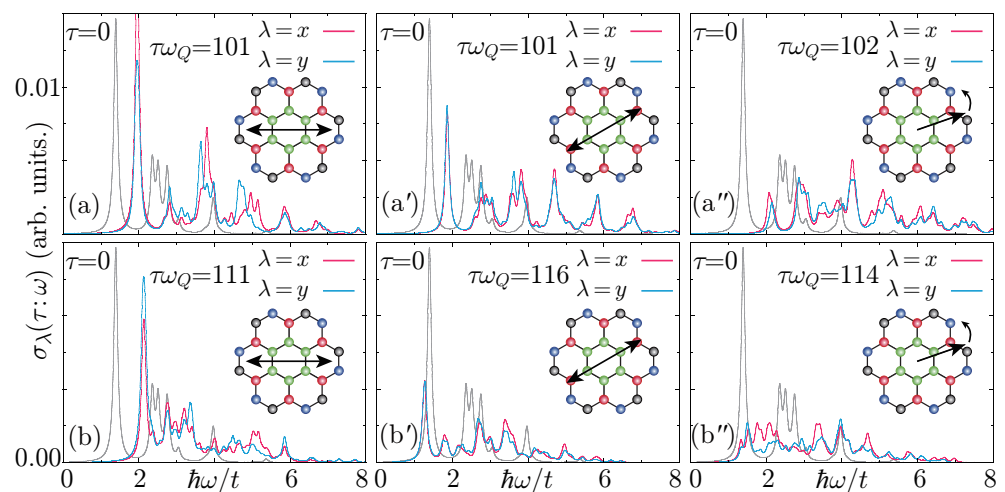**Figure 6.** Instantaneous polarized optical conductivities for the BOW state photoirradiated with linearly polarized light with $\theta = 0$ (**a**,**b**) and $\theta = \pi/6$ (**a′**,**b′**) and circularly polarized light with $\theta = \pi/4$ (**a″**,**b″**).

Second, we focus on the loop currents induced by the linearly polarized light with $\theta = \pi/6$ (Figure 5a′). The loop currents on the first and second benzene rings, third and sixth benzene rings, and fourth and fifth benzene rings, respectively, are circulating pairs in opposite directions to each other. This loop current state is also mirror-symmetric with respect to the polarization plane of $\boldsymbol{E}(\tau)$. Since the induced electric polarizations are small

(Figure 5b′), only the loop currents can be considered to always exist in the photoexcited coronene. In Figure 6a′,b′), the polarization dependence of the optical conductivity is small in comparison with that in Figure 6a.

Finally, we focus on the loop currents induced by the circularly polarized light with $\theta = \pi/4$ (Figure 5a″). No symmetry exists with respect to the loop current structure unlike the case of the linearly polarized light. All the loop current components appear and the heterocentric multiloop structure is formed, but these electric circulations occur at random in both space and time. In addition, the photoexcited coronene is always polarized electrically (Figure 5b″), because the induced P_x and P_y show an asynchronous oscillation due to the initial phase difference in $\boldsymbol{E}(\tau)$. In the optical conductivity spectra (Figure 6a″,b″), characteristics of the CP states, the polarization dependence and the continuous distribution of the oscillator strength, are clearly observed.

Thus, the photoirradiation, that is, the application of the dynamic electric field, induces loop currents accompanied by electric polarizations. These dynamic electric currents and polarizations are both tunable with incident light polarization.

5. Summary and Discussion

We have revealed possible ring current states in coronene under an applied static magnetic field and tracked their dynamic loop current fluctuations induced by an electric field. We find heterocentric multiloop current phases stabilized by an el coupling. The coronene with sufficiently strong el coupling, possibly having heterocentric multiloop currents, shows higher aromaticity. Linearly and circularly polarized lights induce heterocentric two-loop and multiloop currents, respectively. The heterocentric two-loop current occurs in a mirror-symmetric manner, whereas the heterocentric multiloop currents appear at random in both space and time. These dynamic loop currents are strikingly different from a conventional magnetic-field-induced homocentric two-loop current.

Electrically induced loop currents have been investigated in fullerene [35], carbon nanotubes [36,37], and graphene [38] as well. In these systems, an injection of a current by application of a bias voltage gives rise to loop currents inducing magnetic moments. Such an electrical creation of magnetic moments is much more interesting from the viewpoint of applications. For coronene, the $\theta = 0$ linearly polarized light may be useful to make a magnetic moment. In the coronene photoexcited with linearly polarized light with $\theta = 0$, there exists a loop current pair which is mirror-symmetric with respect to the *z-x* plane, as mentioned above. This fact means that the photoexcited system has an antiparallel pair of magnetic moments. On the other hand, in the coronene photoexcited with circularly polarized light with $\theta = \pi/4$, the loop-current-induced magnetic moments are disordered, which leads to the emergence of local paramagnetic moments. The oscillations of these magnetic moments induce magnetic dipole radiation. Such radiation is expected especially in the case of linearly polarized light, which induces coherent oscillation. The photoexcited coronene molecule has a potential application in devices that generate electromagnetic waves. The quantitative estimation of loop-current-induced magnetic moments is an intriguing topic for future research.

Author Contributions: Calculation, analysis, writing, J.O.; calculation, analysis, writing, S.Y. All authors have read and agreed to the published version of the manuscript.

Institutional Review Board Statement: Not applicable.

Informed Consent Statement: Not applicable.

Data Availability Statement: Any data that support the findings of this study are included within the article.

Conflicts of Interest: The authors declare no conflicts of interest.

References

1. Pople, J.A. Molecular orbital theory of aromatic ring currents. *Mol. Phys.* **1958**, *1*, 175. [CrossRef]
2. McWeeny, R. Ring currents and proton magnetic resonance in aromatic molecules. *Mol. Phys.* **1958**, *1*, 311. [CrossRef]
3. Merino, G.; Heine, T.; Seifert, G. The induced Magnetic field in cyclic molecules. *Chem. Eur. J.* **2004**, *10*, 4367. [CrossRef] [PubMed]
4. Gomes, J.A.N.F.; Mallion, R.B. Aromaticity and ring currents. *Chem. Rev.* **2001**, *101*, 1349. [CrossRef]
5. Bühl, M. The relation between endohedral chemical shifts and local aromaticities in fullerenes. *Chem. Eur. J.* **1998**, *4*, 734. [CrossRef]
6. Schulman, J.M.; Disch, R.L. Thermal and magnetic properties of coronene and related molecules. *J. Phys. Chem. A* **1997**, *101*, 9176. [CrossRef]
7. Schleyer, P.V.R.; Maerker, C.; Dransfeld, A.; Jiao, H.; van Eikema Hommes, N.J. Nucleus-independent chemical shifts: A simple and efficient aromaticity probe. *J. Am. Chem. Soc.* **1996**, *118*, 6317. [CrossRef]
8. Steiner, E.; Fowler, P.W.; Jenneskens, L.W. Counter-rotating ring currents in coronene and corannulene. *Angew. Chem. Int. Ed.* **2001**, *40*, 362. [CrossRef]
9. Balaban, A.T.; Bean, D.E.; Fowler, P.W. Patterns of ring current in coronene isomers. *Acta. Chim. Solv.* **2010**, *57*, 507.
10. Randić, M.; Novič, M.; Vračko, M.; Vukičević, D.; Placšć, D. π-electron currents in polycyclic conjugated hydrocarbons: Coronene and its isomers having five and seven member rings. *Int. J. Quant. Chem.* **2012**, *112*, 972. [CrossRef]
11. Kato, T.; Yoshizawa, K.; Yamabe, T. Jahn-Teller effects in the coronene anions and cations. *J. Chem. Phys.* **1999**, *110*, 249. [CrossRef]
12. Kato, T.; Yamabe, T. Electron-intermolecular-phonon coupling and possible superconductivity in negatively charged coronene and corannulene. *J. Chem. Phys.* **2002**, *117*, 2324. [CrossRef]
13. Devos, A.; Lannoo, M. Electron-Phonon coupling for aromatic molecular crystals: Possible consequences for their superconductivity. *Phys. Rev. B* **1998**, *58*, 8236. [CrossRef]
14. Kosugi, T.; Miyake, T.; Ishibashi, S.; Arita, R.; Aoki, H. *Abinitio* electronic structure of solid coronene: Differences from and commonalities to picene. *Phys. Rev. B* **2011**, *84*, 020507(R). [CrossRef]
15. Roth, F.; Bauer, J.; Mahns, B.; Büchner, B.; Kunpfer, M. Electronic structure of undoped and potassium-doped coronene investigated by electron energy-loss spectroscopy. *Phys. Rev. B* **2012**, *85*, 014513. [CrossRef]
16. Kubozono, Y.; Mitamura, H.; Lee, X.; He, X.; Yamanari, Y.; Takahashi, Y.; Suzuki, Y.; Kaji, Y.; Eguchi, R.; Akaike, K.; et al. Metal-intercalated aromatic hydrocarbons: A new class of carbon-based superconductors. *Phys. Chem. Chem. Phys.* **2011**, *13*, 16476. [CrossRef]
17. Malček, M.; Natalia, M.; Cordeiro, D.S. A DFT and QTAIM study of the adsorption of organic molecules over the copper-doped coronene and circumcoronene. *Phys. E* **2018**, *95*, 59. [CrossRef]
18. Joyce, T.; Jaron, A. Ultrafast switching of persistent electron and hole ring currents in a molecule. *Phys. Rev. A* **2023**, *108*, 053114. [CrossRef]
19. Kanno, M.; Kono, H.; Fujimura, Y. Laser-control of ultrafast π-electron ring currents in aromatic molecules: Roles of molecular symmetry and light polarization. *Appl. Sci.* **2018**, *8*, 2347. [CrossRef]
20. Nobusada, K.; Yabana, K. Photoinduced electric currents in ring-shaped molecules by circularly polarized laser pulses. *Phys. Rev. A* **2007**, *75*, 032518. [CrossRef]
21. Zhang, L.; Yamamoto, S. Photoinduced directional and bidirectional phase transitions in bistable linear polycyclic aromatic compounds. *J. Phys. Soc. Jpn.* **2014**, *83*, 064708. [CrossRef]
22. Yamamoto, S. Photoinduced structural phase transitions in polyacene. *J. Phys. Soc. Jpn.* **2011**, *80*, 084713. [CrossRef]
23. Hirano, Y.; Ono, Y. Photogeneration dynamics of a soliton pair in polyacetylene. *J. Phys. Soc. Jpn.* **1998**, *67*, 3835. [CrossRef]
24. Hirano, Y.; Ono, Y. Photogeneration dynamics of nonlinear excitations in polyacetylene. *J. Phys. Soc. Jpn.* **2000**, *69*, 2131. [CrossRef]
25. Subbaswamy, K.R.; Grabowski, M. Bond alternation, on-site Coulomb correlations, and solitons in polyacetylene. *Phys. Rev. B* **1981**, *24*, 2168. [CrossRef]
26. Otsubo, K.; Wakabayashi, Y.; Ohara, J.; Yamamoto, S.; Matsuzaki, H.; Okamoto, H.; Nitta, K.; Uruga, T.; Kitagawa, H. Bottom-up realization of a porous metal-organic nanotubular assembly. *Nat. Mater.* **2011**, *10*, 291. [CrossRef]
27. Funase, K.; Yamamoto, S. Competing ground states of metal-halide ladders. *J. Phys. Soc. Jpn.* **2006**, *75*, 044717. [CrossRef]
28. Steiner, E.; Fowler, P.W.; Jenneskens, L.W.; Acocella, A. Visualisation of counter-rotating ring currents in kekulene. *Chem. Commun.* **2001**, 659–660. [CrossRef]
29. Yamamoto, S. Optical characterization of ground states of polyacene. *Phys. Rev. B* **2008**, *78*, 235205. [CrossRef]
30. Kubo, R. Statistical-Mechanical Theory of Irreversible Processes. I. General Theory and Simple Applications to Magnetic and Conduction Problems. *J. Phys. Soc. Jpn.* **1957**, *12*, 570. [CrossRef]
31. Gammel, J.T.; Saxena, A.; Batistić, I.; Bishop, A.R. Two-band model for halogen-bridged mixed-valence transition-metal complexes. I. Ground state and excitation spectrum. *Phys. Rev. B* **1992**, *45*, 6408. [CrossRef] [PubMed]
32. Ohara, J.; Yamamoto, S. Photocontrollable mixed-valent states in platinum-halide ladder compounds. *Appl. Sci.* **2018**, *8*, 2126. [CrossRef]
33. Ohara, J.; Yamamoto, S. Photoinduced bidirectional magnetism against monodirectional electronics in square-antiprismatic octacyanometalates. *J. Phys. Soc. Jpn.* **2020**, *89*, 093706. [CrossRef]
34. Yan, Y.H.; An, Z.; Wu, C.Q. Dynamics of polaron in a polymer chain with impurities. *Eur. Phys. J. B* **2004**, *42*, 157. [CrossRef]

35. Nakanishi, S.; Tsukada, M. Quantum loop current in a C$_{60}$ molecular bridge. *Phys. Rev. Lett.* **2001**, *87*, 126801. [CrossRef] [PubMed]
36. Tsuji, N.; Takajo, S.; Aoki, H. Large orbital magnetic moments in carbon nanotubes generated by resonant transport. *Phys. Rev. B* **2007**, *75*, 153406. [CrossRef]
37. Wang, B.; Chu, R.; Wang, J.; Guo, H. First-principal calculation of chiral current and quantum self-inductance of carbon nanotubes. *Phys. Rev. B* **2009**, *80*, 235430. [CrossRef]
38. Tsukada, M.; Tagami, K.; Hirose, K.; Kobayashi, N. Theory of quantum conductance of aromatic and molecular bridges. *J. Phys. Soc. Jpn.* **2005**, *74*, 1079. [CrossRef]